PALEOCLIMATE

Phasing of millennial-scale climate variability in the Pacific and Atlantic Oceans

Maureen H. Walczak[1,2]*, Alan C. Mix[1], Ellen A. Cowan[3], Stewart Fallon[2], L. Keith Fifield[2], Jay R. Alder[1,4]†, Jianghui Du[1,5]†, Brian Haley[1]†, Tim Hobern[2]†, June Padman[1]†, Summer K. Praetorius[6]†, Andreas Schmittner[1]†, Joseph S. Stoner[1]†, Sarah D. Zellers[7]†

New radiocarbon and sedimentological results from the Gulf of Alaska document recurrent millennial-scale episodes of reorganized Pacific Ocean ventilation synchronous with rapid Cordilleran Ice Sheet discharge, indicating close coupling of ice-ocean dynamics spanning the past 42,000 years. Ventilation of the intermediate-depth North Pacific tracks strength of the Asian monsoon, supporting a role for moisture and heat transport from low latitudes in North Pacific paleoclimate. Changes in carbon-14 age of intermediate waters are in phase with peaks in Cordilleran ice-rafted debris delivery, and both consistently precede ice discharge events from the Laurentide Ice Sheet, known as Heinrich events. This timing precludes an Atlantic trigger for Cordilleran Ice Sheet retreat and instead implicates the Pacific as an early part of a cascade of dynamic climate events with global impact.

During the last glacial period, the Laurentide Ice Sheet of North America experienced recurrent, unstable millennial-scale retreat events, characterized by episodic iceberg discharge inferred from the presence of apparently ice-rafted detrital sedimentary layers far into the Atlantic Ocean (*1*). These so-called Heinrich events are among the most abrupt climate perturbations of Earth's recent past (*2*). Various triggering mechanisms have been theorized, including reduction of the Atlantic Meridional Overturning Circulation (AMOC) (*3*) warming of subsurface waters (*4*–*6*), internal dynamics of the large Laurentide Ice Sheet (*7*), and/or sea-level rise triggered by episodic failure of another (presumably European) ice sheet (*8*). Regardless of origin, changes in oceanic and atmospheric circulation associated with the Heinrich events correspond to global perturbations, including weak intervals of the Asian monsoon (*9*), and antiphased warming in Antarctica (*10*).

Marine sedimentary records spanning the Northeast Pacific document periods of high ice discharge analogous to the Heinrich events off the west coast of North America, but with uncertain timing and cause (*11*–*14*). Here, on the basis of a detailed radiocarbon chronology in the Gulf of Alaska, we assess the timing of the Pacific ice discharge events from the Cordilleran Ice Sheet and changes in apparent subsurface ocean radiocarbon ages and establish phasing relationships between North Pacific and North Atlantic events. We find that Pacific discharge events and intermediate water ventilation changes precede events in the North Atlantic and are early parts of a dynamic cascade of global climate changes, including Antarctic warming and atmospheric CO_2 rise. We thus reject hypotheses that these North Pacific millennial-scale climate events originate as passive teleconnected responses to the Laurentide/North Atlantic or Antarctic.

During the last glacial period, the Alaskan margin hosted ice streams draining the northwestern limb of the Cordilleran Ice Sheet, evidenced by a series of sedimented troughs crossing the continental shelf (*15*). Although smaller than the Laurentide Ice Sheet, the Cordilleran Ice Sheet at its Last Glacial Maximum (LGM) extent was slightly larger than the modern-day Greenland Ice Sheet (*16*). IODP Site U1419 (59°31.9′N, 144°8.0′W, 690-m water depth; Fig. 1) was drilled on the Gulf of Alaska slope in ~690-m water depth on the continental slope ~75 km seaward of the Bering Glacier, a modern remnant of a major ice stream that may have routed ~15% of drainage from the Cordilleran Ice Sheet (fig. S1). Four drill holes yielded a continuous stratigraphic splice extending back >90 m adjusted core composite depth below seafloor, CCSF-B (*17*).

A Bayesian age model based on 250 ^{14}C measurements of planktic and benthic foraminifera, and limited correlation points beyond the range of ^{14}C (table S1 and fig. S2), indicates that the base of the stratigraphic splice was deposited ~55,000 years before present (yr B.P.) (tables S3 and S4 and Fig. 2). The chronology discussed here is based on calibration of radiocarbon dates using the Marine13 curve (*18*); however, our conclusions are insensitive to calibration on the Marine20 curve (*19*), and that alternate age model is presented and discussed in the supplementary materials. Corrected ages and sediment accumulation rates, and their uncertainties, are resolved in 500-year intervals to ~60,000 yr B.P. (tables S4 and S5). Accumulation rates range from as low as ~10 cm per thousand years (kyr) in mid-Holocene time (average 50 ± 30 cm kyr^{-1}, 0 to 11,700 BP) to peaks of ~800 cm kyr^{-1} during ice discharge events of the latest Pleistocene (average 200 ± 160 cm kyr^{-1}, 12,000 to 50,000 BP; fig. S3).

Each interval of anomalously high sediment accumulation rate off southeast Alaska contains a high concentration of coarse (sand-size or greater) grains not associated with turbidites, interpreted as ice-rafted detritus (IRD) (see materials and methods). Mean IRD mass accumulation rates (MARs) range from zero (indicating that glaciers retreated from the ocean either onto land or behind fjord sills sufficiently shallow to inhibit iceberg fluxes) to as high as 40 g cm^{-2} kyr^{-1}. We name these episodes of high IRD MAR "Siku events" (the Iñupiat/Inuit word for ice, abbreviated here as "S events"), which we define operationally as IRD MAR >12 g cm^{-2} kyr^{-1} averaged over a time span of 500 years or longer. This definition yields events S1 (peak at 17.0 to 18.0 kyr B.P.), S2 (25.0 to 27.0 kyr B.P.), S3 (29.5 to 30.5 kyr B.P.), S4 (39.5 to 42.0 kyr B.P.), and perhaps S5 (~54 to 56 kyr B.P., although the age model and IRD MAR is imprecise in this interval) (Fig. 3 and fig. S9). The Siku events represent a massive influx of icebergs from regional retreat of marine-terminating outlet glaciers from the Cordilleran Ice Sheet. This association is analogous to that of North Atlantic Heinrich events (*20*) and is consistent with evidence for anomalously high sediment fluxes associated with recent tidewater glacier retreat in Alaska (*21*).

The lithology of IRD grains at Site U1419 varies widely, reflecting both proximal sources in the Chugach and St. Elias Ranges drained by the Bering Glacier, as well as more distal sources, including the Alexander terrane of southeast Alaska and western British Columbia (*17*). This diversity of provenance suggests that sediments from the northern Gulf of Alaska integrate ice-rafted detritus from the western Cordilleran ice streams, carried northward and westward by the Alaska Current and Alaska Coastal Current. Meltwater influx likely accelerates these current systems during episodes of rapid ice retreat (*22*). The youngest Siku event (S1) captured in the U1419 marine IRD record coincides with terrestrial cosmogenic-exposure dates for retreat of the western Cordilleran, roughly synchronous on the marine margin from Alaska to southern British Columbia (*23*, *24*).

[1]College of Earth, Ocean, and Atmospheric Sciences, Oregon State University, Corvallis, OR, USA. [2]Australian National University, Canberra ACT. [3]Department of Geological and Environmental Sciences, Appalachian State University, Boone, NC, USA. [4]United States Geological Survey, Corvallis, OR, USA. [5]Department of Earth Sciences, Institute of Geochemistry and Petrology, ETH Zurich, Zurich, Switzerland. [6]United States Geological Survey, Menlo Park, CA, USA. [7]University of Central Missouri, Warrensburg, MO, USA.
*Corresponding author. Email: mo.walczak@oregonstate.edu
†These authors contributed equally to this work.

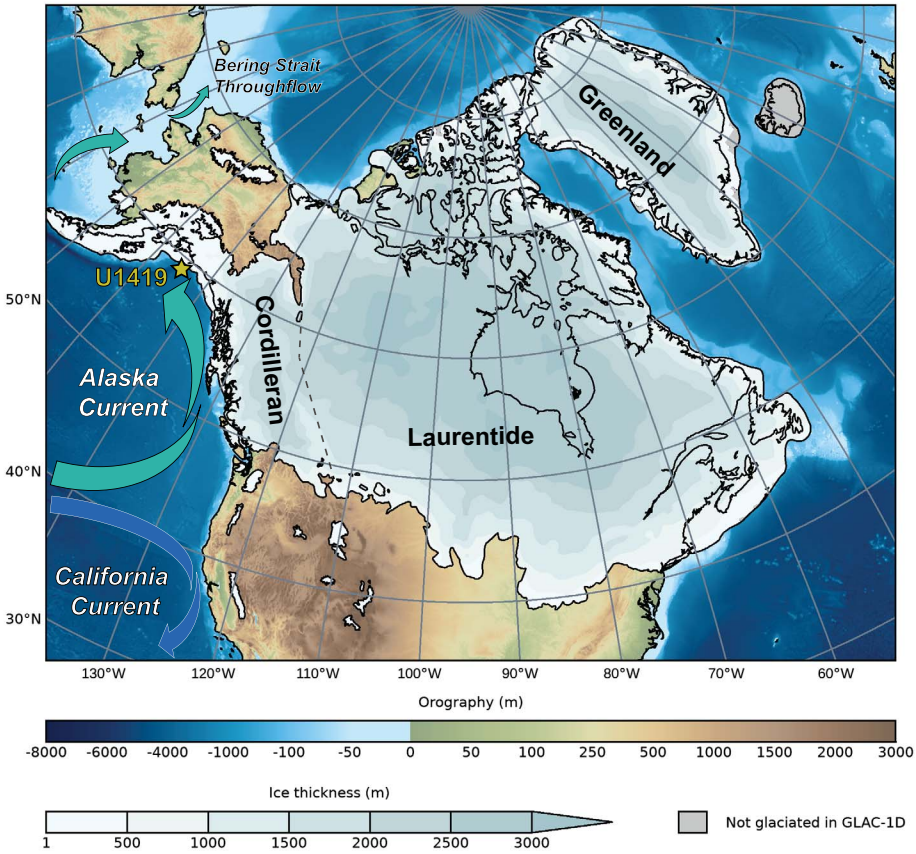

Fig. 1. Map showing study area. Location of International Ocean Discovery Program Expedition 341 Site U1419 (59°31.9′N, 144°8.0′W; 698-m depth) is shown on modern ETOPO1 bathymetry (*58*). The GLAC-1D modeled LGM thickness of the Cordilleran, Laurentide, and Greenland ice sheets is shown (*59*), with margins constrained by the proxy-derived LGM ice extent (*60*). The North American ice sheet saddle separating the Cordilleran from the Laurentide is delineated as a dashed black line. Approximate directions and extent of major northeast Pacific surface currents, including the Alaska Current, California Current, and Bering Strait Throughflow are also shown.

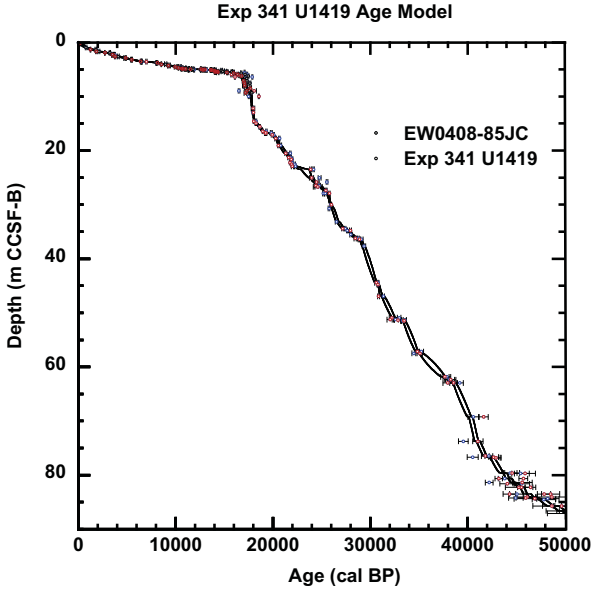

Fig. 2. Bayesian age model for Expedition 341 Site U1419 (see materials and methods) based on the Marine13 calibration curve. The solid lines are the ±1σ error envelope on the age model, shown versus adjusted composite depth below seafloor (CCSF-B) (*17*). All calibrated planktic (blue) and benthic (red) radiocarbon dates are shown. Data from core EW0408-85JC are filled circles (*28*, *33*), whereas data from U1419 are open circles. See materials and methods for Marine20 age model.

The modern water mass at the depth of Site U1419 is at the approximate boundary of North Pacific Intermediate Water [NPIW; an intermediate water mass partially ventilated to the atmosphere in the Sea of Okhotsk) (*25*)] and Pacific Deep Water [PDW; a primary water mass sourced around Antarctica as Circumpolar Deep Water with relatively high preformed ^{14}C age, transited northward from the Southern Ocean near the seafloor as Antarctic Bottom Water and returned southward at mid-depths, mixing with overlying waters but without interacting with the atmosphere (*26*)]. A ^{14}C-depleted water mass expanded through much of the deep Pacific during the most recent glacial termination (*27*), with high apparent ages at intermediate depths approximately coeval with two events of increased benthic reservoir age observed in the Gulf of Alaska (*28*). These events, associated with deglacial increases in atmospheric CO_2, have been inferred to reflect the upward mixing and redistribution of a ^{14}C-depleted deep water mass (*29*, *30*). Evidence from authigenic εNd provides further support for the interpretation of an increased contribution of abyssal Pacific waters to intermediate-depth North Pacific waters at these times (*31*, *32*).

We measured 82 benthic-planktic (B-P) radiocarbon pairs spanning the past ~50,000 yr B.P. at Site U1419, overlapping with and extending 28 paired measurements from <18,000 calibrated ^{14}C years before present (cal yr B.P.) in colocated core EW0408-85JC [59°33.32′N, 144°9.21′W, 682 m (*28*, *33*)] (fig. S2). At this site, an increase in the radiocarbon age of bottom waters relative to the surface (e.g., high B-P values) may indicate (i) decreased circulation rate increasing the true age of subsurface waters; (ii) decreased gas exchange of source waters imparting an apparently high preformed age on the watermass; (iii) shoaling or increased mixing of underlying ^{14}C-deficient deep waters with overlying intermediate waters; and/or (iv) decreased mixing of intermediate waters with the sea surface [for example, through enhanced shallow stratification (*34*)]. The largest B-P age excursions observed here cannot be driven solely by decreases in surface age (for example, by less mixing with underlying older waters or greater effective local gas exchange), as this would require implausible surface-water ages younger than that of the coeval atmosphere (*28*). Thus, substantial increases of B-P age differences must reflect increases in subsurface reservoir ages.

We limit the evaluation of the B-P at Site U1419 to ages <42,000 cal yr B.P. (76.5 m CCSF-B), where analytical precision is sufficient for meaningful interpretation (see materials and methods). The B-P age differences over that interval average 790 ± 340 (1σ) years,

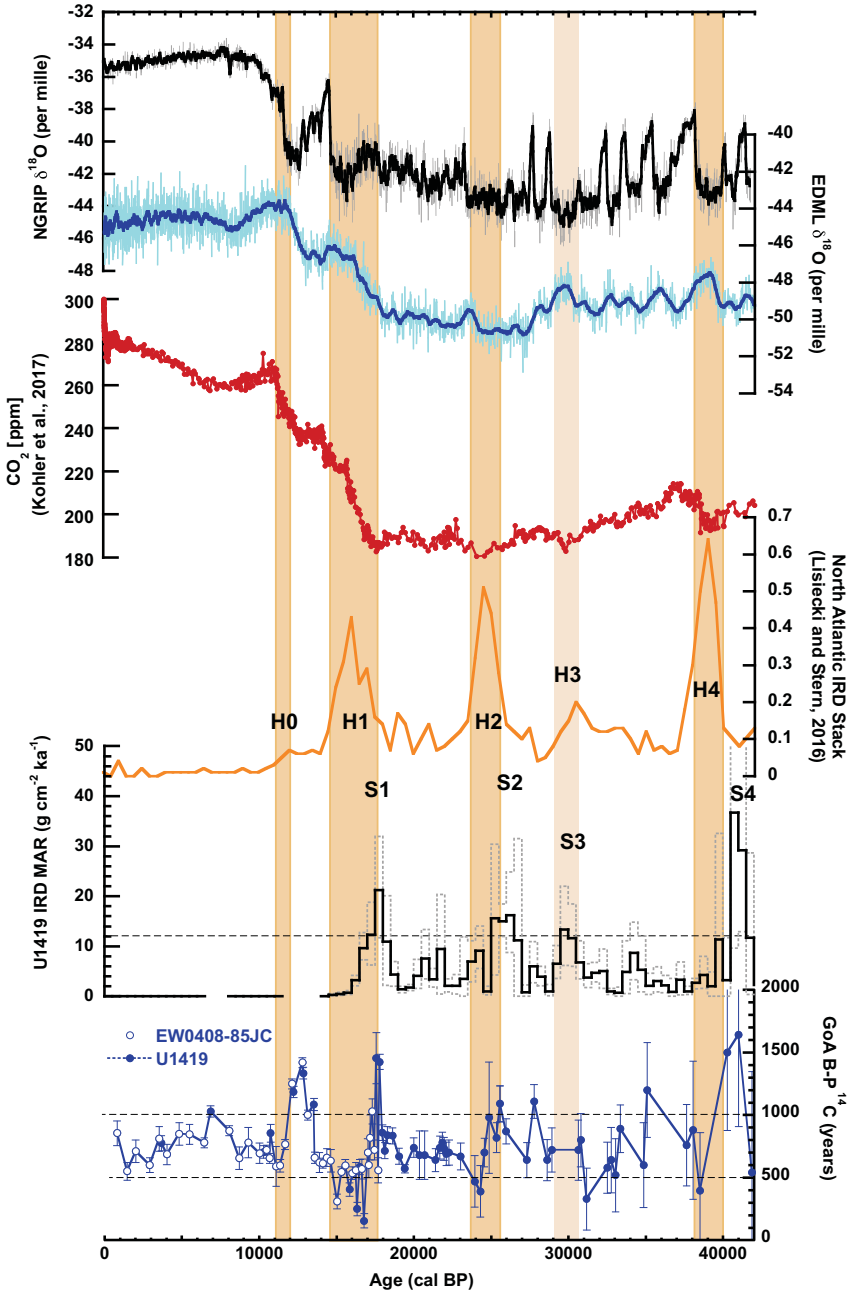

Fig. 3. Global records of climate changes during the latest Pleistocene. Greenland [$\delta^{18}O$ from North Greenland Ice Core Project (NGRIP), black; 100-year smoothing shown in bold] (*61*) and Antarctica ($\delta^{18}O$ from EDML, blue; 100 year smoothing shown in bold) (*62*) are shown on the synchronized AICC2012 time scale (*63*). Global atmospheric CO_2 from ice cores plotted in red (*64*). Atlantic ice-rafted debris stack [normalized units in orange (*65*)] and U1419 IRD MAR calculated over 500-year increments (black) with ± 1σ uncertainty envelope (dashed gray lines). U1419 B-P ^{14}C (blue, ±1σ uncertainty; EW0408-85JC data denoted by open symbols). Timing of the North Atlantic Heinrich events shown in light orange bars; H1 to H4 from synthesis of (*65*), H0 from (*66*). The dashed line on the U1419 IRD panel denotes the level of 12 g cm^{-2} ka^{-1} that define Siku events 1 to 4. The dashed straight lines on the U1419 B-P panel denote 1000 and 500 years; Siku events are associated with regional B-P ^{14}C age differences >1000 years, whereas Heinrich events are associated with values <500 years.

similar to (but with broader range than) the site's average Holocene (<11,700) value of 750 ± 120 (1σ) years (*28*), and estimated modern "pre-bomb" ^{14}C age differences between surface and intermediate waters of 675 ± 90 (1σ) years (*35*). Over the past 42,000 cal yr B.P., four identifiable episodes occurred in which B-P age differences exceed 1000 years (confirmed by two or more B-P pairs), centered at 12,800, 17,700, 25,600, and 40,600 cal yr B.P. (Fig. 3). The older three of these episodes of high B-P are synchronous with Siku events 1, 2, and 4.

A smaller Siku event (S3), potentially associated with H3 near 30,000 cal yr B.P., has no accompanying B-P anomaly at Site U1419 (Fig. 3). However, in this interval, the resolution of the ^{14}C data set is low, so an event may have been missed. The youngest B-P excursion (~12,800 cal yr B.P.), previously identified in nearby core EW0408-85JC (*28*), does not correspond to a Siku event as expressed in IRD, but it is associated with terrestrial ice retreat (*36*–*38*), high meltwater fluxes from land, and adjacent surface ocean cooling (*33*, *39*). By this time, the Cordilleran outlet glaciers had retreated into silled fjords (*36*) that served as sediment traps, leaving little expression of enhanced sediment or IRD fluxes in the open ocean (*40*).

The North Pacific may be sensitive to the Asian monsoon, which provides a net freshwater source that contributes to upper ocean stratification, limiting subsurface ventilation (*41*). High B-P and Siku events are initiated during strong monsoon intervals (higher net freshwater flux to the North Pacific), whereas low B-P events tend to occur in concert with weak monsoons (which are coincident with Atlantic Heinrich events; Fig. 4). Northward heat transport associated with strong monsoons may contribute to net negative mass balance and retreat of the marine margin of the Cordilleran Ice Sheet (*42*). In turn, freshwater discharge from the Cordilleran Ice Sheet can further stratify the northeast Pacific, allow intermediate water reservoir ages to rise as vertical mixing with the surface ocean is suppressed and mixing with the deep ocean is favored, while triggering dynamic responses in the North Atlantic sector (*14*, *39*, *43*, *44*). Chinese Cave $\delta^{18}O$ (*9*) leads Siku events by ~1000 to 3000 years (Fig. 4), reasonable for an ice sheet response to warming. This would seemingly support the hypothesis that low-latitude processes are an important driver of high-latitude climate (*45*).

Antarctic warming, as reconstructed from ice core $\delta^{18}O$, follows within ~1000 years of Siku events, with peak warmth ~2500 years after peak IRD MAR (Figs. 3 and 5). This phasing appears to preclude northward propagation of an Antarctic trigger for Siku events (*3*) but could support a mechanism in which Cordilleran meltwater cools the North Pacific and in turn the North Atlantic, whereby reduction in AMOC triggers Antarctic warming (*43*). Changes in Southern and Pacific Ocean circulation associated with Antarctic warming during the Heinrich events are hypothesized to be related to the release of carbon from the interior ocean, driving some portion of

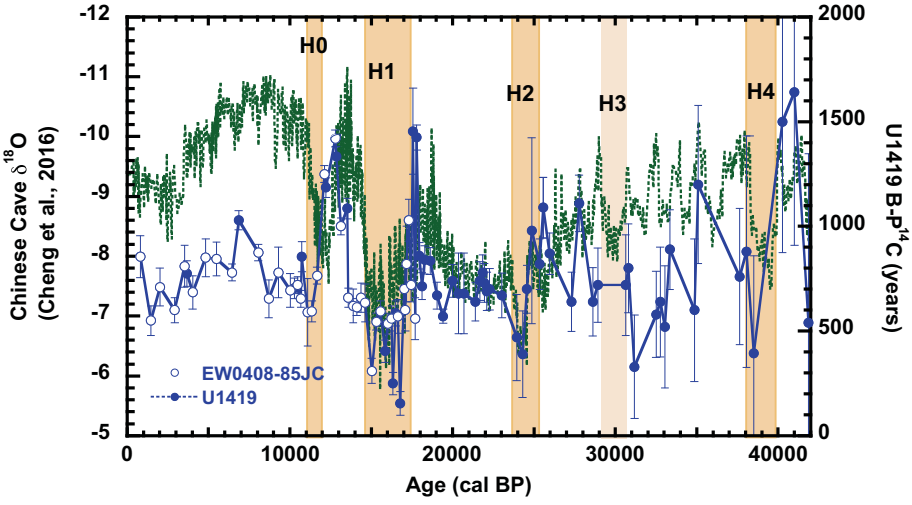

Fig. 4. Paleoclimate connection of the equatorial and high-latitude North Pacific. The B-P ^{14}C record of U1419 (solid blue dots) and its site survey core EW0408-85JC (open blue dots), reflecting changes in the circulation and/or ventilation structure of the intermediate–upper Pacific Ocean, superimposed on the U-Th dated Chinese speleothem $\delta^{18}O$ record interpreted as reflecting strength of the Asian monsoon (green dashed line) (*9*). Episodes of high B-P at U1419, and attendant instability of the Cordilleran (Fig. 4), appear to track periods of strong Asian monsoon. Heinrich events, anomalously low B-P ^{14}C differences, and periods of weak Asian monsoon follow. Timing of the North Atlantic Heinrich events shown in light orange bars; H1 to H4 from synthesis of (*65*), H0 from (*66*).

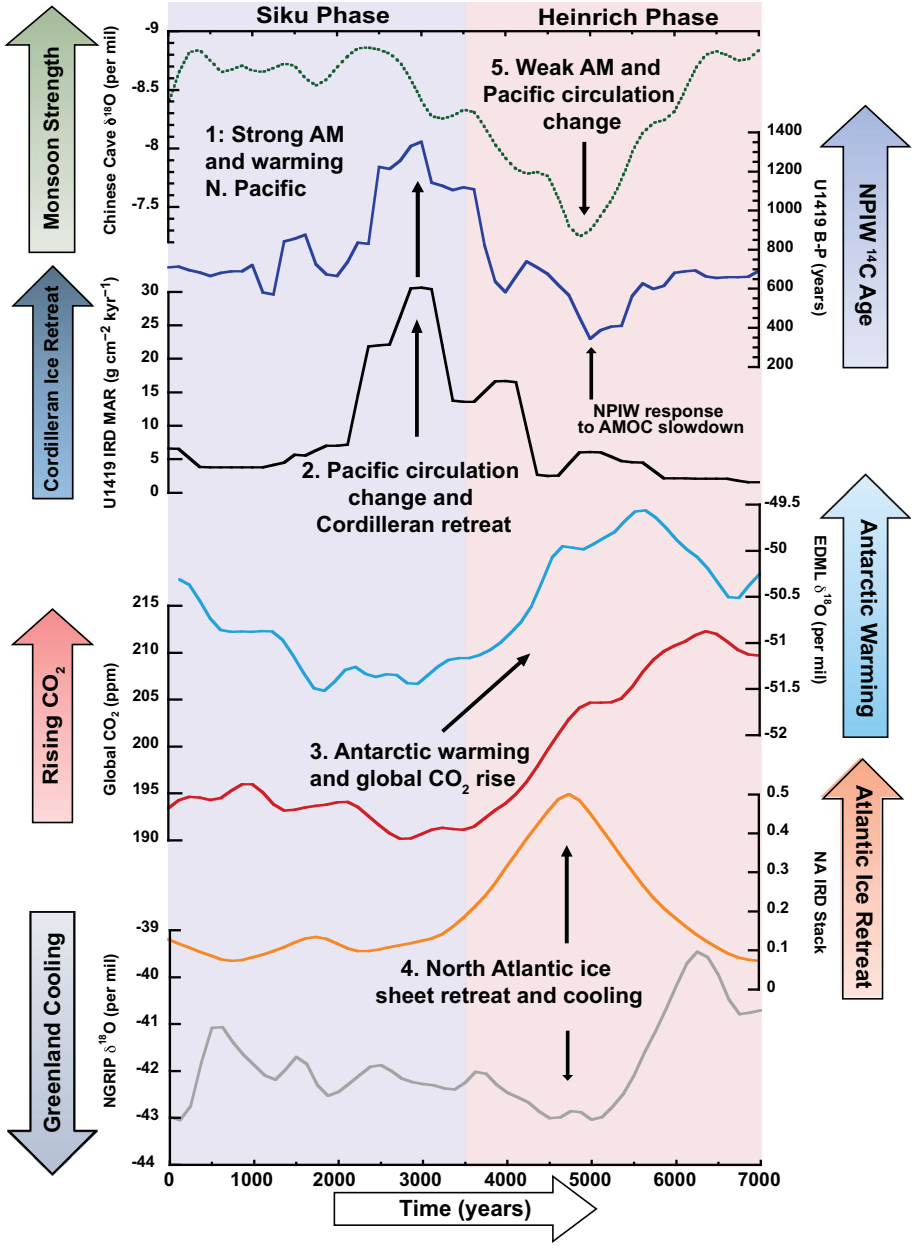

Fig. 5. The progression of global climate anomalies surrounding retreat of the Northern Hemisphere ice sheets over the past ~45,000 cal yr B.P. Canonical events here are averages of the intervals around well-resolved Siku events 1, 2, and 4 aligned on their published chronologies according to the timing of maxima in ice-rafted debris MAR in Site U1419. Each record was then interpolated to 125-year time step and smoothed with a 750-year Gaussian filter. The 7000 years of canonical changes surrounding each event are shown for the Asian monsoon [AM; Chinese Cave speleothem $\delta^{18}O$ (*9*)], Cordilleran ice-rafted debris (IRD) and Northeast Pacific Intermediate Water (NPIW) ventilation age as reconstructed from Site U1419, Antarctic temperature [$\delta^{18}O$ from EDML, blue (*62*)], global atmospheric CO_2 (*64*), North Atlantic IRD (*65*), and Greenland temperature [$\delta^{18}O$ from NGRIP (*61*)]. Ice core records are shown on the synchronized AICC2012 time scale (*63*). Early expression of Northern Hemisphere ice sheet instability (i.e., the "Siku Phase") is seen in the Pacific sector, where intensified Asian monsoon (*9*, *45*) coincides with the start of northeast Pacific ice rafting, and to large positive excursions in the ^{14}C age of NPIW, followed by Antarctic warming and global CO_2 rise. In the "Heinrich Phase," the marine-terminating ice margins of the North Atlantic retreat, generating Heinrich events, and Greenland cools. The Asian monsoon weakens and NPIW ^{14}C ages decrease, likely as a response to a reduction in AMOC (*3*, *9*, *55*).

the following increase in atmospheric CO_2 (*32*, *46*) (Fig. 5).

Atlantic Heinrich events lag Pacific Siku events by 1370 ± 550 years for peak IRD. This phasing precludes teleconnection mechanisms in which Atlantic processes trigger the earlier expression of Pacific millennial-scale climate instability (Fig. 5 and fig. S10). The correspondence of high North Pacific B-P age differences with Siku events similarly precludes their origin as a downstream reduction of Pacific intermediate-water ventilation in response to AMOC suppression during Heinrich events.

Although high B-P age differences in the North Pacific precede Heinrich events, the lowest B-P age differences at Site U1419 co-occur with H0, H1, H2, and H4 and may plausibly reflect the regional response to Heinrich events (Fig. 3). Similar timing for low B-P is found in the northwest Pacific and Bering Sea (*47*–*51*), and may support a hypothesized interocean "see-saw" effect in shallow subsurface ventilation (*52*–*54*). Earth system model results suggest that freshwater input in the North Atlantic during Heinrich events could drive invigorated NPIW production and/or enhanced stratification between NPIW and PDW, both of which would contribute to younger intermediate water age (*55*, *56*).

We have documented correspondence of increased northeast Pacific intermediate water ^{14}C ages and ice-rafted debris delivery during the past 42,000 years. A finely resolved chronology implicates Cordilleran ice retreat (Siku events) as early in a chain of prominent climate events, following strong Asian monsoons but leading the Heinrich events of the North Atlantic, Antarctic warming, and global CO_2 rise (Fig. 5). These observations indicate that the Cordilleran Ice Sheet and North Pacific Ocean play an active role in millennial-scale climate oscillations and preclude direct forcing of Cordilleran ice retreat from Heinrich events. Mechanisms linking Pacific and Atlantic ice retreat events may include atmospheric heat transports and adjustments in the Arctic (*44*), net freshwater transports from the Pacific to the Atlantic when Bering Strait is open (*39*), and/or rapid sea-level rises accompanying ice melt. Precursor retreat of the smaller European ice sheets, posited as a trigger for Laurentide ice purges (8), has since been discounted (*1*). However, the early and rapid Cordilleran ice losses documented here are more likely to influence Atlantic ice sheet retreat. The relative response times of these various interacting systems range from subdecadal (monsoons and atmospheric adjustments), to centuries (smaller Cordilleran ice and water-mass ventilation), to millennia (larger Laurentide ice and interbasin deep circulation), offering a possibility that linkages across a range of time scales could drive auto-oscillating behavior when ice is present as a triggering mechanism (*57*).

REFERENCES AND NOTES

1. S. R. Hemming, *Rev. Geophys.* **42**, RG1005 (2004).
2. W. S. Broecker, *Nature* **372**, 421–424 (1994).
3. P. U. Clark, S. W. Hostetler, K. J. Meissner, N. G. Pisias, A. Schmittner, in *Ocean Circulation: Mechanisms and Impacts - Past and Future Changes of Meridional Overturning*, A. Schmittner, J. C. H. Chiang, S. R. Hemming, Eds., Geophysical Monograph 173 (American Geophysical Union, 2007), pp. 209–246.
4. G. Shaffer, S. M. Olsen, C. J. Bjerrum, *Geophys. Res. Lett.* **31**, L24202 (2004).
5. S. A. Marcott *et al*., *Proc. Natl. Acad. Sci. U.S.A.* **108**, 13415–13419 (2011).
6. J. N. Bassis, S. V. Petersen, L. Mac Cathles, *Nature* **542**, 332–334 (2017).
7. D. R. MacAyeal, *Paleoceanography* **8**, 775–784 (1993).
8. G. C. Bond, R. Lotti, *Science* **267**, 1005–1010 (1995).
9. H. Cheng *et al*., *Nature* **534**, 640–646 (2016).
10. T. Blunier, E. J. Brook, *Science* **291**, 109–112 (2001).
11. A. T. Hewitt, D. Mcdonald, B. D. Bornhold, *Geophys. Res. Lett.* **24**, 3261–3264 (1997).
12. A. C. Mix, D. C. Lund, N. G. Pisias, P. Boden, L. Bornmalm, M. Lyle, J. Pike, in *Mechanisms of Global Climate Change at Millennial Time Scales*, Geophysical Monograph 112 (American Geophysical Union, 1999), pp. 127–148.
13. I. L. Hendy, T. Cosma, *Paleoceanography* **23**, PA2101 (2008).
14. E. Maier *et al*., *Nature* **559**, 241–245 (2018).
15. J. M. Swartz, S. P. S. Gulick, J. A. Goff, *Geochem. Geophys. Geosyst.* **16**, 165–177 (2015).
16. J. Seguinot, I. Rogozhina, A. P. Stroeven, M. Margold, J. Kleman, *Cryosphere* **10**, 639–664 (2016).
17. J. M. Jaeger *et al.*, and the Expedition 341 Scientists (Integrated Ocean Drilling Program, College Station, TX, 2014). doi:10.2204/iodp.pr.341.2014.
18. P. J. Reimer *et al*., *Radiocarbon* **55**, 1869–1887 (2013).
19. T. J. Heaton *et al*., *Radiocarbon* **62**, 779–820 (2020).
20. S. J. Marshall, M. R. Koutnik, *Paleoceanography* **21**, PA2021 (2006).
21. M. N. Koppes, B. Hallet, *Geology* **30**, 47–50 (2002).
22. T. C. Royer, B. Finney, *Oceanography (Wash. D.C.)* **33**, (2020).
23. C. M. Darvill, B. Menounos, B. M. Goehring, O. B. Lian, M. W. Caffee, *Geophys. Res. Lett.* **45**, 9710–9720 (2018).
24. A. J. Lesnek, J. P. Briner, C. Lindqvist, J. F. Baichtal, T. H. Heaton, *Sci. Adv.* **4**, eaar5040 (2018).
25. L. D. Talley, *J. Phys. Oceanogr.* **23**, 517–537 (1993).
26. L. D. Talley, *Oceanography (Wash. D.C.)* **26**, 80–97 (2013).
27. T. M. Marchitto, S. J. Lehman, J. D. Ortiz, J. Flückiger, A. van Geen, *Science* **316**, 1456–1459 (2007).
28. M. Davies-Walczak *et al*., *Earth Planet. Sci. Lett.* **397**, 57–66 (2014).
29. E. L. Sikes, C. R. Samson, T. P. Guilderson, W. R. Howard, *Nature* **405**, 555–559 (2000).
30. L. Skinner *et al*., *Earth Planet. Sci. Lett.* **411**, 45–52 (2015).
31. C. Basak, E. E. Martin, K. Horikawa, T. M. Marchitto, *Nat. Geosci.* **3**, 770–773 (2010).
32. J. Du, B. A. Haley, A. C. Mix, M. H. Walczak, S. K. Praetorius, *Nat. Geosci.* **11**, 749–755 (2018).
33. M. H. Davies *et al*., *Paleoceanography* **26**, PA2223 (2011).
34. S. Khatiwala, F. Primeau, M. Holzer, *Earth Planet. Sci. Lett.* **325-326**, 116–125 (2012).
35. R. M. Key *et al*., *Global Biogeochem. Cycles* **18**, GB4031 (2004).
36. B. Menounos *et al*., *Science* **358**, 781–784 (2017).
37. J. P. Briner, D. S. Kaufman, *J. Quat. Sci.* **23**, 659–670 (2008).
38. D. S. Kaufman, R. Scott Anderson, F. S. Hu, E. Berg, A. Werner, *Quat. Sci. Rev.* **29**, 1445–1452 (2010).
39. S. K. Praetorius *et al*., *Sci. Adv.* **6**, eaay2915 (2020).
40. E. A. Cowan *et al*., *Bull. Geol. Soc. Am.* **122**, 1067–1080 (2010).
41. J. Emile-Geay, *J. Geophys. Res.* **108**, 3178 (2003).
42. S. Hostetler, N. Pisias, A. Mix, *Quat. Sci. Rev.* **25**, 1168–1185 (2006).
43. D. M. Roche, A. P. Wiersma, H. Renssen, *Clim. Dyn.* **34**, 997–1013 (2010).
44. S. Praetorius, M. Rugenstein, G. Persad, K. Caldeira, *Nat. Commun.* **9**, 3124 (2018).
45. J. W. Beck *et al*., *Science* **360**, 877–881 (2018).
46. M. Sarnthein, B. Schneider, P. M. Grootes, *Clim. Past* **9**, 2595–2614 (2013).
47. N. Ahagon, *Geophys. Res. Lett.* **30**, 2097 (2003).
48. Y. Okazaki *et al*., *Science* **329**, 200–204 (2010).
49. L. Max *et al*., *Clim. Past* **10**, 591–605 (2014).
50. J. W. B. Rae *et al*., *Paleoceanography* **29**, 1–23 (2014).
51. W. R. Gray *et al*., *Nat. Geosci.* **11**, 1 (2018).
52. D. C. Lund, *Earth Planet. Sci. Lett.* **381**, 52–62 (2013).
53. A. T. Kotilainen, N. J. Shackleton, *Nature* **377**, 323–326 (1995).
54. O. A. Saenko, A. Schmittner, A. J. Weaver, *J. Clim.* **17**, 2033–2038 (2004).
55. M. O. Chikamoto *et al*., *Deep. Res. Part II Top. Stud. Oceanogr.* **61–64**, 114–126 (2012).
56. X. Gong *et al*., *Nat. Commun.* **10**, 656 (2019).
57. M. Crucifix, *Philos. Trans. A Math. Phys. Eng. Sci.* **370**, 1140–1165 (2012).
58. C. Amante, B. W. Eakins, ETOPO1 Global Relief Model converted to PanMap layer format. NOAA-National Geophysical Data Center, PANGAEA (2009). https://doi.org/10.1594/PANGAEA.769615.
59. W. R. Peltier, D. F. Argus, R. Drummond, *J. Geophys. Res. Solid Earth* **120**, 450–487 (2015).
60. R. McNeely, A. S. Dyke, J. R. Southon, *Geol. Surv. Canada Open File* **5049** (2006).
61. K. K. Andersen *et al*., *Nature* **431**, 147–151 (2004).
62. L. Augustin *et al*., *Nature* **429**, 623–628 (2004).
63. D. Veres *et al*., *Clim. Past* **9**, 1733–1748 (2013).
64. P. Köhler, C. Nehrbass-Ahles, J. Schmitt, T. F. Stocker, H. Fischer, *Earth Syst. Sci. Data* **9**, 363–387 (2017).
65. L. E. Lisiecki, J. V. Stern, *Paleoceanography* **31**, 1368–1394 (2016).
66. C. Pearce *et al*., *Paleoceanography* **30**, 1613–1624 (2015).

ACKNOWLEDGMENTS

We are grateful to the crew and shipboard science party of IODP Expedition 341, as well as the curators at the IODP Gulf Coast Repository. **Funding:** This work was supported by the Australian Research Council (FS100100076), the Australia-New Zealand IODP Commission, the U.S. Science Support Program and Consortium for Ocean Leadership, the National Science Foundation (0242084, 0602395, 0728315, 1103538, 1204204, 1357529, 1360894, 1434945, 1436903, 1502754, 1924215 1929486), and the American Australian Association. **Author contributions:** M.W., A.M., and S.F. designed study, generated ^{14}C data, and analyzed datasets. E.C. generated and aided in interpretation of IRD data. K.F. generated dates for oldest ^{14}C samples. J.P., T.H., and J.D. prepared samples for ^{14}C analysis. S.Z. prepared species-specific benthic ^{14}C samples for evaluation of down-slope transport. J.A. contributed to interpretation of modeled ice sheet behavior and figure creation, including Cordilleran meltwater input. A.S. contributed to modeling of ocean radiocarbon reservoir age. M.W., A.M., S.F., E.C., S.P., J.S., J.D., B.H., and S.Z. contributed to writing of the paper. **Competing interests:** The authors declare no competing interests. **Data and materials availability:** All data are available in the main text or the supplementary materials.

SUPPLEMENTARY MATERIALS

science.sciencemag.org/content/370/6517/716/suppl/DC1
Materials and Methods
Figs. S1 to S15
Tables S1 to S10
References (*67*–*77*)

26 December 2019; accepted 17 September 2020
Published online 1 October 2020
10.1126/science.aba7096

Science

Phasing of millennial-scale climate variability in the Pacific and Atlantic Oceans

Maureen H. WalczakAlan C. MixEllen A. CowanStewart FallonL. Keith FifieldJay R. AlderJianghui DuBrian HaleyTim HobernJune PadmanSummer K. PraetoriusAndreas SchmittnerJoseph S. StonerSarah D. Zellers

Science, 370 (6517), • DOI: 10.1126/science.aba7096

Calving cousins

Walczak *et al.* report that increases in Pacific Ocean ventilation and periods of rapid production of icebergs from the Cordilleran Ice Sheet during the last glacial period preceded episodic iceberg discharges into the Atlantic Ocean (see the Perspective by Jaeger and Shevenell). Marine sediments from the Gulf of Alaska show that increases in vertical mixing of the ocean there correspond with intense iceberg calving from the ice sheet that covered much of high-latitude western North America and that these changes occurred before the analogous Heinrich events in the North Atlantic. Thus, these Pacific climate system reorganizations may have been an early part of a cascade of dynamic climate events with global repercussions.

Science, this issue p. 716; see also p. 662